https://doi.org/10.3311/PPci.23010
Creative Commons Attribution

Periodica Polytechnica Civil Engineering

A Substructure-based Model Updating Method to Damage Detection for Large-scale Structures

Jiexin Yu[1], Wei Lin[2*], Xin Chen[1], Benfei Xie[3]

[1] Faculty of Engineering, Fujian Jiangxia University, Xiyuangong Road 2., 350108 Fuzhou, Fujian, China
[2] Faculty of Civil Engineering, Fuzhou University, Xue Yuan Road 2., 350108 Fuzhou, Fujian, China
[3] Fuzhou Guiwu Real Estate Co., Ltd., Wentang Road 237., Jinan District, 350011 Fuzhou, Fujian, China
[*] Corresponding author, e-mail: cewlin@fzu.edu.cn

Received: 17 July 2023, Accepted: 20 October 2023, Published online: 03 January 2024

Abstract

The health monitoring and damage detection of structures are major scientific issues that the civil engineering discipline, which made great achievements in the 20th century, has bequeathed to the 21st century. Despite the installation of health monitoring systems in many large structures, implementing damage detection through finite element model updating is often time-consuming or even infeasible due to the size of the model and the presence of numerous uncertain parameters. To address this issue, this paper proposes a substructure-based model updating method. The entire structure is divided into substructures with reduced degrees of freedom, allowing for the simplification of the motion equation by employing only a small number of low-order modes from each substructure. Consequently, the analysis scale of the structure is effectively reduced. The discarded higher modes are compensated by residual modes to ensure the accuracy of structural response and sensitivity. Subsequently, a damage identification program substructure-based model updating is developed, which is applied to component mode synthesis and damage identification for large structures. By precisely detecting damage in critical areas, accurate diagnosis and evaluation of the global structural safety are achieved. The results validate the implementation, computational efficiency, and accuracy of the proposed substructure-based model updating method. This approach shifts the focus from model updating of the entire structure to model updating of substructures, with the aim of fundamentally resolving the technical challenge of accurate damage detection of large and complex structures. Furthermore, it provides theoretical support for the practical application of damage detection in large civil structures.

Keywords

damage detection, FE model updating, substructure, component mode synthesis

1 Introduction

During the entire service life of structures, their structural performance gradually degrades over time due to environmental influences, resulting in varying degrees of damage such as cracks and deformations. The traditional approach is to conduct maintenance after localized failure or damage occurs in the structure, known as post-maintenance. However, carrying out post-maintenance on structures that have suffered significant damage and performance degradation will significantly increase maintenance costs, often with minimal benefit. By utilizing health monitoring technology to detect structural defects as early as possible, timely repairs can be undertaken before the structural performance reaches its limit state. This proactive approach of "treating minor issues to prevent major problems" ensures structural safety, extends the service life, and facilitates predictive maintenance.

Health monitoring technology was first introduced in the field of civil engineering around 1970. Currently, numerous large-span bridges and buildings have been equipped with health monitoring systems, both domestically and internationally. Examples include the Golden Gate Bridge in the United States [1], the Akashi Kaikyo Bridge in Japan [2], and in China, structures such as the Tsing Ma Bridge [3], the Guangzhou TV Tower [4], and the Shenzhen Ping-An Financial Center [5]. However, large structures like the Guangzhou TV Tower generate over 200,000 monitoring data in a single day and up to 100 million in a year, making it extremely challenging

Cite this article as: Yu, J., Lin, W., Chen, X., Xie, B. "A Substructure-based Model Updating Method to Damage Detection for Large-scale Structures", Periodica Polytechnica Civil Engineering, 2024. https://doi.org/10.3311/PPci.23010

to diagnose structural safety conditions accurately and swiftly from such a vast amount of monitoring data [6–8].

In the past two decades, there has been significant interest in utilizing dynamic property changes for damage detection [9–14]. The finite element model updating technique involves adjusting model parameters iteratively based on measured data, aiming to minimize the differences between theoretical and measured values. This iterative process aims to obtain a finite element model that closely represents the actual structure, treating it as an optimization problem. Shi et al. [15] proposed a sensitivity-based model updating method to detect and quantify damage in two-dimensional truss structures using incomplete measurement modes. Wu and Li [16] conducted model updating for Nanjing TV Station using frequency and vibration mode analysis. Weber and Paultre [17] performed experiments to identify damage in three-dimensional towers using a sensitivity-based model updating method. These studies demonstrate that the damage identification method based on finite element model updating can achieve accurate damage localization and quantification, making it one of the most direct and effective approaches for structural health assessment.

However, for large and complex engineering structures with finite element models consisting of thousands or even millions of degrees of freedom, traditional model updating methods result in a significant number of matrix operations, posing great challenges to the solution process. For instance, Papadimitriou and Papadioti [18] conducted a study on the Egnatia Odos highway bridge in Greece. The bridge's finite element model consisted of 562,101 degrees of freedom and 97,636 elements, and an intact structure was performed for modal updating, taking approximately one month and seven days to complete the computation. Xia et al. [19] carried out model updating for the Balla Balla Bridge in Western Australia, which had a finite element model with 4,200 degrees of freedom and 1,200 elements. The convergence required 155 iterations and approximately 420 hours to achieve. Duan et al. [20] developed a finite element model for the Tsing Ma Bridge, which included about 1.2 million degrees of freedom, and it took 5 hours to solve the first 100 eigen solutions of the model. Despite the increasing computational power, which has created favorable conditions for finite element model updating, achieving precise model updating and damage identification for large structures remains challenging in practical applications.

To address the challenges, this paper proposes the application of the substructuring method for damage identification, employing a local-to-global analysis approach by dividing the entire structure into substructures for separate analysis. In comparison to the global structure, substructures exhibit higher sensitivity to local element damage, as well as fewer degrees of freedom and parameters requiring updated. This approach effectively reduces the computational scale and expedites the convergence of the optimization process. By analyzing and detecting individual substructures, the need for repetitive calculations on the entire structure is circumvented, thereby significantly reducing the computational burden associated with dynamic analysis and finite element model updating for large structures. Through the extraction of key information, the structural safety status can be accurately determined, providing an effective method for the health monitoring of large structures during service.

2 Free interface component mode synthesis method

The free interface component mode synthesis (CMS) method, developed by Craig and Chang [21], is based on the concept of dividing a complex structure into substructures with free interfaces. The method involves performing modal analysis for each substructure to extract their respective eigenmodes, which is then combined to represent the global structure. Take Fig. 1 as an example, where the global structure with degrees of freedom N is divided into two substructures a and b for illustration. The degrees of freedom of substructures a and b are N_a and N_b, respectively. For the purpose of this illustration, we will focus on substructure a. The undamped dynamic equation for substructure a can be defined by:

$$\boldsymbol{M}^{(a)}\ddot{\boldsymbol{x}}^{(a)} + \boldsymbol{K}^{(a)}\boldsymbol{x}^{(a)} = \boldsymbol{f}^{(a)}. \tag{1}$$

In this paper, superscript "(a)" is used to denote the item corresponding to substructure a. The mass and stiffness matrices, denoted as $\boldsymbol{M}^{(a)}$ and $\boldsymbol{K}^{(a)}$ respectively, have a size of $N_a \times N_a$. The displacement and acceleration vectors, represented by $\boldsymbol{x}^{(a)}$ and $\ddot{\boldsymbol{x}}^{(a)}$, respectively, have a size of $N_a \times 1$. The load vector, denoted as $\boldsymbol{f}^{(a)}$, contains the connecting loads from neighboring substructures. A coordinate transformation relating physical coordinates to modal coordinates can be expressed as:

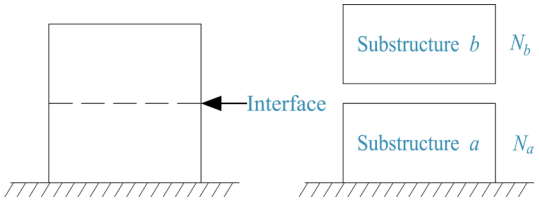

Fig. 1 Global structure and substructures

$$\boldsymbol{x}^{(a)} = \boldsymbol{\Phi}^{(a)} \boldsymbol{p}^{(a)}, \tag{2}$$

where $\boldsymbol{\Phi}^{(a)}$ is the eigenvector matrix of the substructure, with a size of $N_a \times N_a$; $\boldsymbol{p}^{(a)}$ represents the modal coordinate. According to the lower and higher modes, Eq. (2) can be rewritten as:

$$\boldsymbol{x}^{(a)} = \begin{bmatrix} \boldsymbol{\Phi}_l^{(a)} & \boldsymbol{\Phi}_h^{(a)} \end{bmatrix} \begin{Bmatrix} \boldsymbol{p}_l^{(a)} \\ \boldsymbol{p}_h^{(a)} \end{Bmatrix} = \boldsymbol{\Phi}_l^{(a)} \boldsymbol{p}_l^{(a)} + \boldsymbol{\Phi}_h^{(a)} \boldsymbol{p}_h^{(a)}, \tag{3}$$

where $\boldsymbol{\Phi}_l^{(a)}$ and $\boldsymbol{\Phi}_h^{(a)}$ represents the lower and higher modes with a size of $N_a \times N_{al}$ and $N_a \times N_{ah}$.

To reduce the computational complexity while maintaining the accuracy of modal synthesis, the method retains only a limited number of lower modes. The discarded higher modes can be compensated for using residual flexibility modes, with the interface force acting as the corresponding coordinate. This expression can be approximated as:

$$\boldsymbol{x}^{(a)} = \boldsymbol{\Phi}_l^{(a)} \boldsymbol{p}_l^{(a)} + \boldsymbol{\psi}_h^{(a)} \boldsymbol{f}_J^{(a)} = \begin{bmatrix} \boldsymbol{\Phi}_l^{(a)} & \boldsymbol{\psi}_h^{(a)} \end{bmatrix} \begin{Bmatrix} \boldsymbol{p}_l^{(a)} \\ \boldsymbol{f}_J^{(a)} \end{Bmatrix}, \tag{4}$$

where $\boldsymbol{f}_J^{(a)}$ is the interface force with a size of $N_J \times 1$ and N_J is the number of interface DOFs; $\boldsymbol{\psi}_h^{(a)}$ is the residual flexibility, can be expressed as:

$$\boldsymbol{\psi}_h^{(a)} = \boldsymbol{\Phi}_h^{(a)} \left(\boldsymbol{\Omega}_h^{(a)} \right)^{-1} \left(\boldsymbol{\Phi}_h^{(a)} \right)^T \left(\boldsymbol{B}^{(a)} \right)^T. \tag{5}$$

Given that the flexibility matrix can be decomposed into lower and higher modes as:

$$\begin{aligned} &\left(\boldsymbol{K}^{(a)} \right)^{-1} = \boldsymbol{\Phi}^{(a)} \left(\boldsymbol{\Omega}^{(a)} \right)^{-1} \left(\boldsymbol{\Phi}^{(a)} \right)^T \\ &= \boldsymbol{\Phi}_l^{(a)} \left(\boldsymbol{\Omega}_l^{(a)} \right)^{-1} \left(\boldsymbol{\Phi}_l^{(a)} \right)^T + \boldsymbol{\Phi}_h^{(a)} \left(\boldsymbol{\Omega}_h^{(a)} \right)^{-1} \left(\boldsymbol{\Phi}_h^{(a)} \right)^T. \end{aligned} \tag{6}$$

We define:

$$\begin{aligned} &\boldsymbol{G}^{(a)} = \left(\boldsymbol{K}^{(a)} \right)^{-1} \left(\boldsymbol{B}^{(a)} \right)^T \\ &= \boldsymbol{\Phi}_l^{(a)} \left(\boldsymbol{\Omega}_l^{(a)} \right)^{-1} \left(\boldsymbol{\Phi}_l^{(a)} \right)^T \left(\boldsymbol{B}^{(a)} \right)^T \\ &+ \boldsymbol{\Phi}_h^{(a)} \left(\boldsymbol{\Omega}_h^{(a)} \right)^{-1} \left(\boldsymbol{\Phi}_h^{(a)} \right)^T \left(\boldsymbol{B}^{(a)} \right)^T = \boldsymbol{\psi}_a^{(a)} + \boldsymbol{\psi}_h^{(a)}, \end{aligned} \tag{7}$$

where $\boldsymbol{\psi}_a^{(a)}$ and $\boldsymbol{\psi}_h^{(a)}$ represent the contributions of the lower and higher modes to the flexibility matrix, respectively. $\boldsymbol{\psi}_h^{(a)}$ can be calculated as:

$$\boldsymbol{\psi}_h^{(a)} = \boldsymbol{G}^{(a)} - \boldsymbol{\psi}_a^{(a)}. \tag{8}$$

If a substructure is floating, then the inverse of $\boldsymbol{K}^{(a)}$ is unavailable. In such case, the rigid-body modes $\boldsymbol{\Phi}_R^{(a)}$ are disregarded. The derivation of the equation mentioned here is quite complex and cannot be fully explained in this context. Detailed information can be found in [21] for a comprehensive understanding. The flexibility matrix with rigid-body modes can be written as

$$\boldsymbol{G}^{(a)} = \left(\Re^{(a)} \right)^T \boldsymbol{G}_c^{(a)} \Re^{(a)} \left(\boldsymbol{B}^{(a)} \right)^T, \tag{9}$$

$$\Re^{(a)} = \boldsymbol{I}^{(a)} - \boldsymbol{M}^{(a)} \boldsymbol{\Phi}_R^{(a)} \left(\boldsymbol{\Phi}_R^{(a)} \right)^T. \tag{10}$$

When Eq. (4) is substituted into Eq. (1) and pre-multiplying both sides by $\begin{bmatrix} \boldsymbol{\Phi}_l^{(a)} & \boldsymbol{\psi}_h^{(a)} \end{bmatrix}^T$, one obtains:

$$\tilde{\boldsymbol{M}}^{(a)} \ddot{\boldsymbol{p}}^{(a)} + \tilde{\boldsymbol{K}}^{(a)} \boldsymbol{p}^{(a)} = \begin{bmatrix} \boldsymbol{\Phi}_l^{(a)} & \boldsymbol{\psi}_h^{(a)} \end{bmatrix}^T \left(\boldsymbol{B}^{(a)} \right)^T \boldsymbol{f}_J^{(a)}, \tag{11}$$

where:

$$\begin{aligned} &\tilde{\boldsymbol{M}}^{(a)} = \begin{bmatrix} \boldsymbol{I}_l^{(a)} & \boldsymbol{0} \\ \boldsymbol{0} & \boldsymbol{M}_G^{(a)} \end{bmatrix}, \ \tilde{\boldsymbol{K}}^{(a)} = \begin{bmatrix} \boldsymbol{\Omega}_l^{(a)} & \boldsymbol{0} \\ \boldsymbol{0} & \boldsymbol{K}_G^{(a)} \end{bmatrix}, \\ &\boldsymbol{p}^{(a)} = \begin{Bmatrix} \boldsymbol{p}_l^{(a)} \\ \boldsymbol{f}_J^{(a)} \end{Bmatrix}. \end{aligned} \tag{12}$$

The size of the equations presented above is $(N_a + N_J)$. $\boldsymbol{\Omega}_l$ and $\boldsymbol{\Omega}_h$ are eigenvalue matrices for the lower and higher modes, respectively; $\boldsymbol{I}$ is the identity matrix; $\boldsymbol{B}^{(a)}$ is the Boolean matrix; $\boldsymbol{M}_G^{(a)}$ and $\boldsymbol{K}_G^{(a)}$ are the residual mass and residual stiffness matrices, respectively. They are computed as:

$$\boldsymbol{M}_G^{(a)} = \left(\boldsymbol{\psi}_h^{(a)} \right)^T \boldsymbol{M}^{(a)} \boldsymbol{\psi}_h^{(a)}, \ \boldsymbol{K}_G^{(a)} = \left(\boldsymbol{\psi}_h^{(a)} \right)^T \boldsymbol{K}^{(a)} \boldsymbol{\psi}_h^{(a)}. \tag{13}$$

To assemble two substructures together for representing the dynamics of the entire structure, it can be block-diagonally assembled as:

$$\begin{aligned} &\begin{bmatrix} \tilde{\boldsymbol{M}}^{(a)} & \boldsymbol{0} \\ \boldsymbol{0} & \tilde{\boldsymbol{M}}^{(b)} \end{bmatrix} \begin{Bmatrix} \ddot{\boldsymbol{p}}^{(a)} \\ \ddot{\boldsymbol{p}}^{(b)} \end{Bmatrix} + \begin{bmatrix} \tilde{\boldsymbol{K}}^{(a)} & \boldsymbol{0} \\ \boldsymbol{0} & \tilde{\boldsymbol{K}}^{(b)} \end{bmatrix} \begin{Bmatrix} \boldsymbol{p}^{(a)} \\ \boldsymbol{p}^{(b)} \end{Bmatrix} \\ &= \begin{bmatrix} \begin{bmatrix} \boldsymbol{\Phi}_l^{(a)} & \boldsymbol{\psi}_h^{(a)} \end{bmatrix}^T \left(\boldsymbol{B}^{(a)} \right)^T & \boldsymbol{0} \\ \boldsymbol{0} & \begin{bmatrix} \boldsymbol{\Phi}_l^{(b)} & \boldsymbol{\psi}_h^{(b)} \end{bmatrix}^T \left(\boldsymbol{B}^{(b)} \right)^T \end{bmatrix} \\ &\times \begin{Bmatrix} \boldsymbol{f}_J^{(a)} \\ \boldsymbol{f}_J^{(b)} \end{Bmatrix} = \begin{Bmatrix} \boldsymbol{F}^{(a)} \\ \boldsymbol{F}^{(b)} \end{Bmatrix}. \end{aligned} \tag{14}$$

Similarly, the superscript "(*b*)" represents the item associated with substructure *b*. Substructures *a* and *b* are connected at the common interface. The compatibility of displacements and equilibrium of perpendicular normal forces at the interface between substructure *a*

and substructure *b*. And they can be expressed through Eqs. (15) and (16):

$$\boldsymbol{x}_J^{(a)} = \boldsymbol{x}_J^{(b)}, \tag{15}$$

$$\boldsymbol{f}_J^{(a)} = -\boldsymbol{f}_J^{(b)}. \tag{16}$$

Given $\boldsymbol{x}_J^{(a)} = \boldsymbol{B}^{(a)}\boldsymbol{x}^{(a)}$ and $\boldsymbol{x}_J^{(b)} = \boldsymbol{B}^{(b)}\boldsymbol{x}^{(b)}$, by substituting Eq. (4) into Eq. (15), we have:

$$\boldsymbol{B}^{(a)}\left(\boldsymbol{\Phi}_l\boldsymbol{p}_l + \boldsymbol{\psi}_h\boldsymbol{f}_J\right)^{(a)} = \boldsymbol{B}^{(b)}\left(\boldsymbol{\Phi}_l\boldsymbol{p}_l + \boldsymbol{\psi}_h\boldsymbol{f}_J\right)^{(b)}. \tag{17}$$

By combining Eqs. (16) and (17), the interface force can be determined as follows:

$$\begin{aligned}\boldsymbol{f}_J^{(a)} &= -\boldsymbol{f}_J^{(b)} \\ &= \left[\left(\boldsymbol{B}\boldsymbol{\psi}_h\right)^{(a)} + \left(\boldsymbol{B}\boldsymbol{\psi}_h\right)^{(b)}\right]^{-1}\left[\left(\boldsymbol{B}\boldsymbol{\Phi}_l\boldsymbol{p}_l\right)^{(b)} - \left(\boldsymbol{B}\boldsymbol{\Phi}_l\boldsymbol{p}_l\right)^{(a)}\right].\end{aligned} \tag{18}$$

Hence, the modal coordinates of substructures can be transformed into the modal coordinates associated with the lower modes as follows:

$$\boldsymbol{p} = \begin{Bmatrix}\boldsymbol{p}^{(a)} \\ \boldsymbol{p}^{(b)}\end{Bmatrix} = \begin{Bmatrix}\boldsymbol{p}_l^{(a)} \\ \boldsymbol{f}_J^{(a)} \\ \boldsymbol{p}_l^{(b)} \\ \boldsymbol{f}_J^{(b)}\end{Bmatrix} = \begin{bmatrix}\boldsymbol{I} & \boldsymbol{0} \\ \boldsymbol{A} & \boldsymbol{D} \\ \boldsymbol{0} & \boldsymbol{I} \\ -\boldsymbol{A} & -\boldsymbol{D}\end{bmatrix}\begin{Bmatrix}\boldsymbol{p}_l^{(a)} \\ \boldsymbol{p}_l^{(b)}\end{Bmatrix} = \boldsymbol{T}\boldsymbol{q}, \tag{19}$$

where:

$$\begin{aligned}\boldsymbol{A} &= -\left[\left(\boldsymbol{B}\boldsymbol{\psi}_h\right)^{(a)} + \left(\boldsymbol{B}\boldsymbol{\psi}_h\right)^{(b)}\right]^{-1}\left(\boldsymbol{B}\boldsymbol{\Phi}_l\right)^{(a)}, \\ \boldsymbol{D} &= \left[\left(\boldsymbol{B}\boldsymbol{\psi}_h\right)^{(a)} + \left(\boldsymbol{B}\boldsymbol{\psi}_h\right)^{(b)}\right]^{-1}\left(\boldsymbol{B}\boldsymbol{\Phi}_l\right)^{(b)},\end{aligned} \tag{20}$$

where $\boldsymbol{T}$ is the transformation matrix of size $(N_{al} + N_{bl} + 2N_J) \times (N_{al} + N_{bl})$ and $\boldsymbol{q}$ represents the modal coordinate associated with the lower modes of the two substructures, with a size of $(N_{al} + N_{bl}) \times 1$. Substituting Eq. (19) into Eq. (14) and pre-multiplying both sides by $\boldsymbol{T}^T$, we obtain:

$$\boldsymbol{M}^*\ddot{\boldsymbol{p}} + \boldsymbol{K}^*\boldsymbol{q} = 0, \tag{21}$$

where:

$$\boldsymbol{M}^* = \boldsymbol{T}^T\tilde{\boldsymbol{M}}\boldsymbol{T}, \quad \boldsymbol{K}^* = \boldsymbol{T}^T\tilde{\boldsymbol{K}}\boldsymbol{T}. \tag{22}$$

Equation (21) is the final eigensystem equation of the assembled global structure with a size of $(N_{al} + N_{bl})$. Since the interface forces always appear in pairs when there is no external force, the right-hand term of Eq. (21) is zero. Assuming that its eigensolutions are $\boldsymbol{\Omega}^*$ and $\boldsymbol{\Phi}^*$, the eigenvalues of the original system are $\boldsymbol{\Omega}^*$ and the eigenvectors can be transformed as:

$$\boldsymbol{\Phi} = \begin{bmatrix}\boldsymbol{\Phi}^{(a)} & \\ & \boldsymbol{\Phi}^{(b)}\end{bmatrix}\boldsymbol{T}\boldsymbol{\Phi}^* = \boldsymbol{\Phi}^p\boldsymbol{T}\boldsymbol{\Phi}^*, \tag{23}$$

where superscript '*p*' denotes the diagonal assembly of the substructural matrices. Since only a few lower modes of each substructure are included, the size of the reduced eigenequation $(N_{al} + N_{bl})$. is much smaller compared to the global eigenequation with size *N*. This allows us to avoid solving the large eigenequation, leading to computational efficiency.

3 Finite element model updating method based on substructure

Structural damage cause variations in structural responses and identifying damage by detecting variations in structural dynamic properties is a typical approach to solving inverse problems. The finite element model updating method uses structural parameters as the updating variables and employs iterative optimization to reproduce the actual dynamic properties of the structure. It is extensively employed in engineering for solving inverse problems [22]. The relationship between structural responses and structural parameters can be established through a first-order Taylor expansion, given by:

$$\boldsymbol{R}_e - \boldsymbol{R}_o = \boldsymbol{S}\left(\boldsymbol{r}_u - \boldsymbol{r}_o\right), \tag{24}$$

where $\boldsymbol{R}_e$ and $\boldsymbol{R}_o$ are the experimental and analytical responses of the structure, respectively; $\boldsymbol{r}_u$ and $\boldsymbol{r}_o$ represent the corresponding structural parameter vectors. The matrix $\boldsymbol{S}$ is a sensitivity matrix that relates the change in the structural parameters to changes in the vibration properties. It can be obtained by calculating the derivatives of the structural responses with respect to the structural parameters. In practical structures, damage typically affects the stiffness matrix, in the subsequent derivations, it is assumed that damage causes a reduction in the stiffness of one or more elements in the structure.

During the optimization process, the elemental parameters in the analytical model are iteratively modified to match the experimental vibration properties. When the structure has a large number of degrees of freedom, traditional model updating methods based on the system matrices of the global structure can become computationally challenging. In each iteration, it is necessary to recalculate the eigensolutions and eigensensitivity matrix of the analytical model, which can be time-consuming and complex. The sensitivity matrix of the element level damage identification for more precise damage localization and quantification can be obtained by using the substructuring

method. According to Eq. (21), the eigenequation of the i-th mode (i = 1, 2, …, N) representation as:

$$\left(\boldsymbol{K}^{*}-\boldsymbol{M}^{*}\lambda_{i}\right)\boldsymbol{\Phi}_{i}^{*}=0. \tag{25}$$

Differentiating Eq. (25) with respect to parameter r one obtains:

$$\frac{\partial\left(\boldsymbol{K}^{*}-\boldsymbol{M}^{*}\lambda_{i}\right)}{\partial r}\boldsymbol{\Phi}_{i}^{*}+\left(\boldsymbol{K}^{*}-\boldsymbol{M}^{*}\lambda_{i}\right)\frac{\partial\boldsymbol{\Phi}_{i}^{*}}{\partial r}=0. \tag{26}$$

Pre-multiplying both sides of Eq. (30) by $\left(\boldsymbol{\Phi}_{i}^{*}\right)^{T}$, we have:

$$\begin{aligned}&\left(\boldsymbol{\Phi}_{i}^{*}\right)^{T}\frac{\partial\left(\boldsymbol{K}^{*}-\boldsymbol{M}^{*}\lambda_{i}\right)}{\partial r}\boldsymbol{\Phi}_{i}^{*}\\&+\left(\boldsymbol{\Phi}_{i}^{*}\right)^{T}\left(\boldsymbol{K}^{*}-\boldsymbol{M}^{*}\lambda_{i}\right)\frac{\partial\boldsymbol{\Phi}_{i}^{*}}{\partial r}=0.\end{aligned} \tag{27}$$

$\left(\boldsymbol{K}^{*}-\boldsymbol{M}^{*}\lambda_{i}\right)\boldsymbol{\Phi}_{i}^{*}=0$ and $(\boldsymbol{K}^{*}-\boldsymbol{M}^{*}\lambda_{i})$ is symmetric. Hence, Eq. (27) can be simplified as:

$$\left(\boldsymbol{\Phi}_{i}^{*}\right)^{T}\frac{\partial\left(\boldsymbol{K}^{*}-\boldsymbol{M}^{*}\lambda_{i}\right)}{\partial r}\boldsymbol{\Phi}_{i}^{*}=0. \tag{28}$$

Considering that the normalization property of $\boldsymbol{\Phi}_{i}^{*}$, the derivative of eigenvalue λ_{i} can be expressed by:

$$\frac{\partial\lambda_{i}}{\partial r}=\left(\boldsymbol{\Phi}_{i}^{*}\right)^{T}\frac{\partial\boldsymbol{K}^{*}}{\partial r}\boldsymbol{\Phi}_{i}^{*}. \tag{29}$$

According to Eq. (23), the i-th eigenvector of the global structure can be written as:

$$\boldsymbol{\Phi}_{i}=\boldsymbol{\Phi}^{p}\boldsymbol{T}\boldsymbol{\Phi}_{i}^{*}. \tag{30}$$

Differentiating Eq. (30) with respect to parameter r one obtains:

$$\frac{\partial\boldsymbol{\Phi}_{i}}{\partial r}=\frac{\partial\boldsymbol{\Phi}^{p}}{\partial r}\boldsymbol{T}\boldsymbol{\Phi}_{i}^{*}+\boldsymbol{\Phi}^{p}\boldsymbol{T}\frac{\partial\boldsymbol{\Phi}_{i}^{*}}{\partial r}, \tag{31}$$

where $\partial\boldsymbol{\Phi}^{p}/\partial r$ is the derivative of the eigenvector of the substructure that contains parameter r, and it can be calculated within the substructure. $\partial\boldsymbol{\Phi}^{*}/\partial r$ can be expressed by following Nelson's method [23] as:

$$\frac{\partial\boldsymbol{\Phi}_{i}^{*}}{\partial r}=\boldsymbol{v}_{i}+c_{i}\boldsymbol{\Phi}_{i}^{*}, \tag{32}$$

where c_{i} is the participation factor. By substituting Eq. (32) into Eq. (26), we have:

$$\left(\boldsymbol{K}^{*}-\boldsymbol{M}^{*}\lambda_{i}\right)\left(\boldsymbol{v}_{i}+c_{i}\boldsymbol{\Phi}_{i}^{*}\right)=-\frac{\partial\left(\boldsymbol{K}^{*}-\boldsymbol{M}^{*}\lambda_{i}\right)}{\partial r}\boldsymbol{\Phi}_{i}^{*}. \tag{33}$$

Given that $\left(\boldsymbol{K}^{*}-\boldsymbol{M}^{*}\lambda_{i}\right)\boldsymbol{\Phi}_{i}^{*}=0$, Eq. (33) can be simplified as:

$$\boldsymbol{X}_{i}\boldsymbol{v}_{i}=\boldsymbol{Y}_{i}, \tag{34}$$

where:

$$\boldsymbol{X}_{i}=\left(\boldsymbol{K}^{*}-\boldsymbol{M}^{*}\lambda_{i}\right),\ \boldsymbol{Y}_{i}=-\frac{\partial\left(\boldsymbol{K}^{*}-\boldsymbol{M}^{*}\lambda_{i}\right)}{\partial r}\boldsymbol{\Phi}_{i}^{*}. \tag{35}$$

Vector $\boldsymbol{v}_{i}$ can be solved using Eq. (34). The solution of c_{i} can be calculated from the orthogonal condition of the eigenvector:

$$\left(\boldsymbol{\Phi}_{i}^{*}\right)^{T}\boldsymbol{M}^{*}\boldsymbol{\Phi}_{i}^{*}=1. \tag{36}$$

Differentiating Eq. (36) with respect to r yields:

$$\begin{aligned}&\frac{\partial\left(\boldsymbol{\Phi}_{i}^{*}\right)^{T}}{\partial r}\boldsymbol{M}^{*}\boldsymbol{\Phi}_{i}^{*}+\left(\boldsymbol{\Phi}_{i}^{*}\right)^{T}\frac{\partial\boldsymbol{M}^{*}}{\partial r}\boldsymbol{\Phi}_{i}^{*}\\&+\left(\boldsymbol{\Phi}_{i}^{*}\right)^{T}\boldsymbol{M}^{*}\frac{\partial\boldsymbol{\Phi}_{i}^{*}}{\partial r}=0.\end{aligned} \tag{37}$$

By substituting Eq. (32) into Eq. (37), given $\partial\boldsymbol{M}^{*}/\partial r=0$, yields Eq. (38):

$$\left[\left(\boldsymbol{v}_{i}\right)^{T}+c_{i}\left(\boldsymbol{\Phi}_{i}^{*}\right)^{T}\right]\boldsymbol{M}\boldsymbol{\Phi}_{i}^{*}+\left(\boldsymbol{\Phi}_{i}^{*}\right)^{T}\boldsymbol{M}^{*}\left(\boldsymbol{v}_{i}+c_{i}\boldsymbol{\Phi}_{i}^{*}\right)=0. \tag{38}$$

The participation factor c_{i} can be obtained as:

$$c_{i}=-\frac{1}{2}\left(\left(\boldsymbol{v}_{i}\right)^{T}\boldsymbol{M}^{*}\boldsymbol{\Phi}_{i}^{*}+\left(\boldsymbol{\Phi}_{i}^{*}\right)^{T}\boldsymbol{M}^{*}\boldsymbol{v}_{i}\right). \tag{39}$$

The final form for the first-order derivative of $\boldsymbol{\Phi}_{i}^{*}$ with respect to parameter r is expressed by Eq. (40):

$$\frac{\partial\boldsymbol{\Phi}_{i}^{*}}{\partial r}=\boldsymbol{v}_{i}-\frac{1}{2}\left[\left(\boldsymbol{v}_{i}\right)^{T}\boldsymbol{M}^{*}\boldsymbol{\Phi}_{i}^{*}+\left(\boldsymbol{\Phi}_{i}^{*}\right)^{T}\boldsymbol{M}^{*}\boldsymbol{v}_{i}\right]\boldsymbol{\Phi}_{i}^{*}. \tag{40}$$

4 Numerical simulation of component mode synthesis

4.1 Numerical example

A numerical study of a large-scale frame structure is conducted, as depicted in Fig. 2. This structure consists of 12 floors, each with a height of 2.9 m. It features 4 spans in the X-direction, with each span measuring 8.4 m, as well as 3 spans in the Y-direction, with each span having a length of 5.7 m. The node numbers indicated in Fig. 2 correspond to the global structure, which comprises 260 nodes. The bottom 20 nodes are fixed supports, resulting in a total of 1440 degrees of freedom. The total number of components is 612. The beam and column components are I-beams, where the cross-section parameters of the beam are h = 0.4 m, b = 0.2 m, and t = 0.02 m, and the

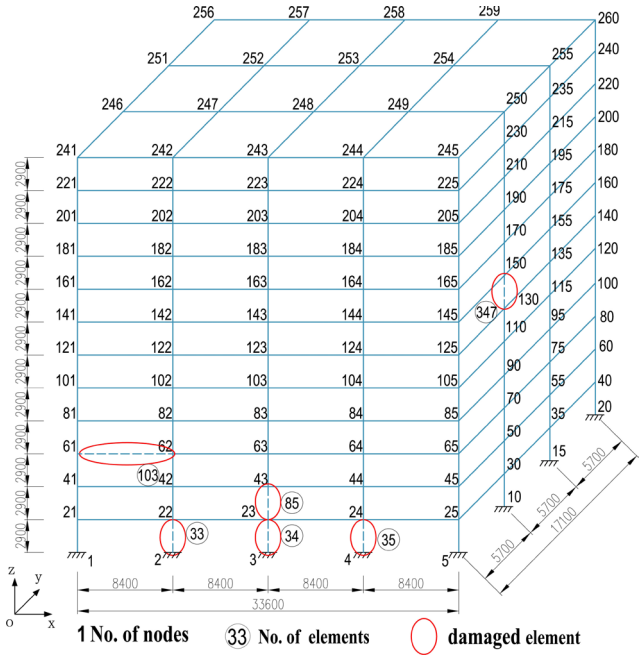

Fig. 2 Large-scale frame structure (unit: mm)

cross-section parameters of the column are h = 0.4 m, b = 0.4 m, t = 0.02 m. The elements are constructed from Q235 steel, and their nonlinear material behavior is characterized by a bilinear kinematic hardening model along with the Von Mises yield criterion. The slope of the elastic segment is taken as the elastic modulus of the steel material, and the slope of the strengthening segment is taken as 1/100 of the elastic segment. Specifically, the material properties of the steel are defined as follows: Young's modulus = 2.1 × 10^5 MPa, Mass density = 7800 kg/m^3, Poisson's ratio v = 0.3.

The stiffness matrix and mass matrix of both the frame model and the substructures are established using the MATLAB [24] code. This preparation enables further CMS and model updating. To validate the results obtained from MATLAB [24], modal analysis is performed using the finite element model in ANSYS [25], and the first 3 mode shapes are depicted in Fig. 3.

To evaluate accuracy, the relative change *Diff* of frequency f and the modal assurance criterion (MAC) are utilized. A MAC value of 0 implies that two sets of modes ϕ are completely unrelated, while a value of 1 indicates complete correlation between vibration modes. The specific formula is as follows:

$$Diff\left(f_i^d, f_i^o\right) = \left|\frac{f_i^d - f_i^o}{f_i^o}\right|, \tag{41}$$

$$\mathrm{MAC}\left(\phi_d, \phi_o\right) = \frac{\left|\phi_d{}^T \phi_o\right|^2}{\phi_d{}^T \phi_d \phi_o{}^T \phi_o}. \tag{42}$$

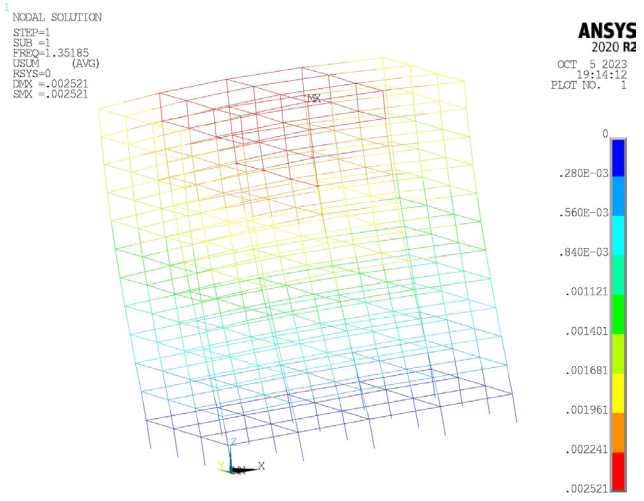

(a)

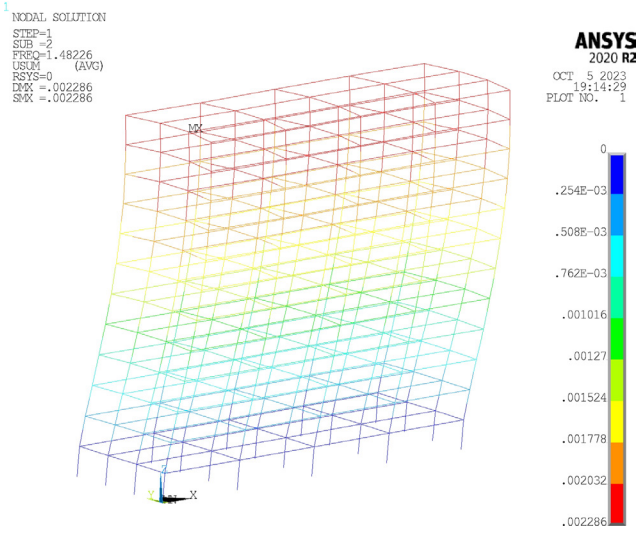

(b)

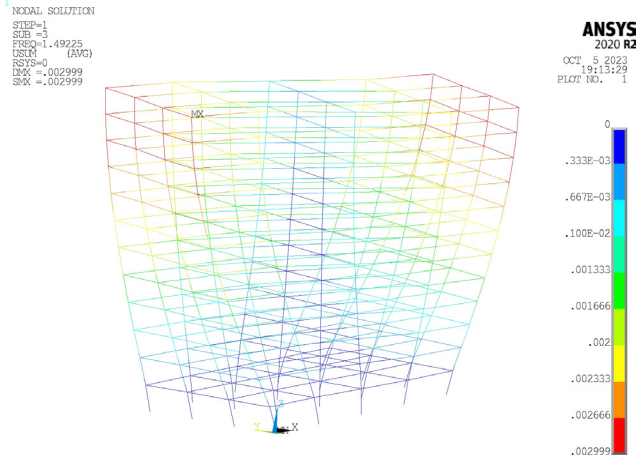

(c)

Fig. 3 The first 3 mode shapes of the FE model for the structure (unit: m); (a) Mode 1; (b) Mode 2; (c) Mode 3

Table 1 lists the corresponding frequencies and MAC values, obtained from both MATLAB [24] and ANSYS [25]. A comparison between the two sets of data reveals that the modal analysis conducted using MATLAB [24] is highly accurate. The maximum discrepancy among the first 10 modal frequencies is only 0.9451%, and the MAC values for each mode are nearly equal to one, indicating that MATLAB [24] accurately replicates its structural dynamic behavior of the system.

4.2 Effectiveness of component mode synthesis

In order to accurately capture the global modal parameters, it is essential to establish a reasonable criterion for modal truncation to select the relevant modes of the substructure. By substituting Eq. (3) into Eq. (1) and pre-multiplying both sides by $(\boldsymbol{\Phi}^{(a)})^T$, we obtain Eq. (43):

$$\boldsymbol{I}_h^{(a)}\ddot{\boldsymbol{p}}_h^{(a)} + \boldsymbol{\Omega}_h^{(a)}\boldsymbol{p}_h^{(a)} = \left(\boldsymbol{\Phi}_h^{(a)}\right)^T \left(\boldsymbol{B}^{(a)}\right)^T \boldsymbol{f}_J^{(a)}. \tag{43}$$

For example, the subsystem vibrates at frequency ω and amplitude b, that is, $\boldsymbol{p}_h = b\sin(\omega t)$ and $\ddot{\boldsymbol{p}}_h = -\omega^2 b\sin(\omega t)$. The first term in Eq. (41) is much smaller than the second term, thus it can be concluded as:

$$\left|\omega^2 b\sin(\omega t)\right| << \left|\omega_h^2 b\sin(\omega t)\right|, \tag{44}$$

$$\lambda << \lambda_h. \tag{45}$$

Based on the derivation, it can be inferred that the discarded higher-order eigenvalues of the substructures, which must be significantly larger than the eigenvalues to be solved for the global structure.

To facilitate the analysis, the global structure is evenly divided into three substructures, as depicted in Fig. 4. Following to the CMS method, the global structure is divided into substructures and all interface constraints are removed. This decomposition of the entire structural system into several independent substructures enables entirely independent research on the dynamic analysis of each substructure. In Fig. 4, the substructure 1 is fixed and constrained at the bottom, while the substructures 2 and 3 are floating and unconstrained at the interfaces 1 and 2. Detailed information regarding the global structure and each substructure can be found in Table 2.

In this example, the first 10 modes of the global structure are of interest. Through modal analysis of the global structure, it has been determined that the 10th eigenvalue is 705.388 rad^2/s^2. To assess the impact of the number of reserved modes on the CMS, three schemes of retained modes have been selected. Each scheme preserves eigenvalues of the substructures that are 10, 20, and 50 times greater than the eigenvalues to be solved for the global

Table 1 Frequency and MAC of the FE model and MATLAB model

Mode No.	Frequency (f)			MAC
	ANSYS (Hz)	MATLAB (Hz)	*Diff* (%)	
1	1.3518	1.3498	0.1480	1.0000
2	1.4823	1.4858	0.2361	0.9999
3	1.4923	1.4897	0.1742	0.9999
4	1.9382	1.9480	0.5056	0.9996
5	1.9501	1.9655	0.7897	0.9994
6	2.5076	2.5313	0.9451	0.9992
7	2.9625	2.9847	0.7494	0.9998
8	2.9871	3.0144	0.9139	0.9995
9	4.0046	4.0013	0.0824	1.0000
10	4.2131	4.2270	0.3299	0.9997

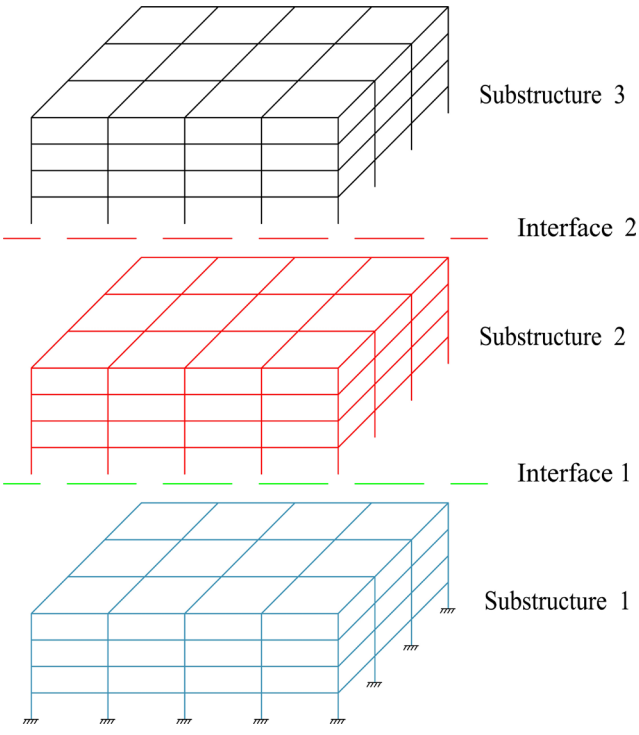

Fig. 4 Substructures

Table 2 The information of the global structure and substructures

Structural information		Global structure	Sub 1	Sub 2	Sub 3
Number of nodes		260	100	100	100
Number of DOFs		1440	480	600	600
Number of elements		612	204	204	204
Number of interface nodes			20	40	20
Number of retained modes	Scheme 1	1440	49	68	68
	Scheme 2		76	97	97
	Scheme 3		96	137	137

structure. These schemes are presented in Table 2 as Schemes 1, 2, and 3, respectively.

Figs. 5 and 6 illustrates the modal error between the reconstructed structural calculation results obtained using the free interface CMS method and the calculation results of the complete finite element model. It is evident that as the reserved modal order of the substructure increases, the calculation accuracy after synthesis improves significantly. Most frequency relative errors for the three modal retention schemes are below 10^{-2}, demonstrating good accuracy. When the number of reserved modes is increased to Scheme 3, the maximum frequency relative error is only 8.778×10^{-5}. Regarding vibration modes, Scheme 1 exhibits a minimum MAC value of 0.9837 for the 7th order vibration mode. The first 10 orders of MAC in the other two schemes are greater than 0.9957, while Scheme 3 attains a minimum MAC value of 0.9996. These results indicate that the reconstructed structure obtained through the free interface CMS method aligns closely with the calculation results of the original global structure, ensuring the accuracy of the proposed CMS method in calculating eigensolutions.

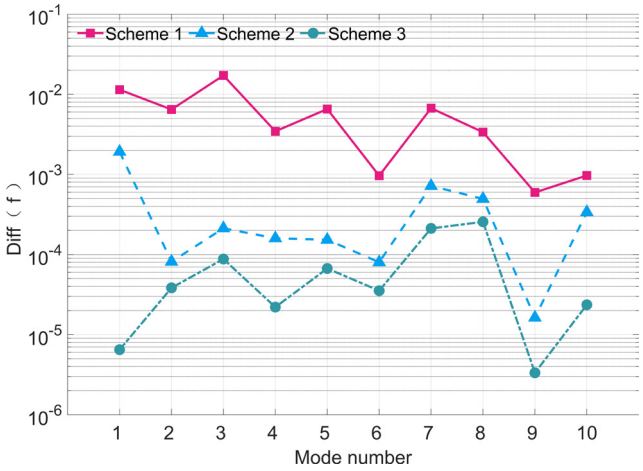

Fig. 5 Relative error of frequency

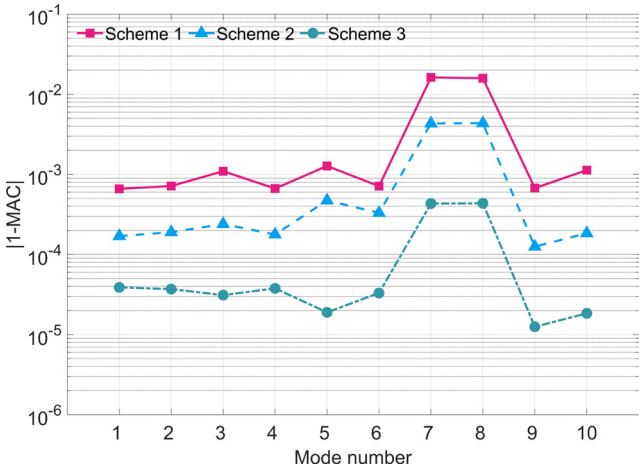

Fig. 6 Error of MAC

Referring to Table 2, it can be observed that compared to the number of degrees of freedom in the global model, the restructuring of the structure using the CMS technique significantly reduces the number of degrees of freedom. Scheme 3, which retains the highest number of modes, accounts for only about 25.7% of the original structure, while maintaining high calculation accuracy. This reduction in degrees of freedom will greatly facilitate the practical application of the proposed sub-structuring method in finite element model updating.

4.3 Impact of local damage on eigenparameters

To investigate the sensitivity of the eigenparameters of the global structure and substructures to local damage, damage is simulated by reducing the bending stiffness of the element. The specific damage scenarios are listed in Table 3, and the detailed location is depicted in Fig. 2. Fig. 7 presents the variations in eigenparameters of the global structure and substructures as the damage degree increases from 50% to 80% at the same damaged element for both Case 1 and Case 2.

Based on the calculation results, it can be observed that the degree of change in structural eigenparameters is significantly positively correlated with the extent of damage. For instance, when the damage degree is 50%, the relative change of the first 10 frequencies of the global structure does not exceed 0.015, and the average of the first 20 MAC values of eigenvectors is 0.997. As the damage degree increases to 80%, the maximum relative change of the first 10 frequencies is 0.033, and the average of the first 20 MAC values of eigenvectors decreases to 0.735. These findings demonstrate that as the damage degree increases, the eigenparameters exhibit a higher rate of change, indicating greater sensitivity to damage. However, the overall amplitude of change in the global eigenparameters by local damage is not significant.

The analysis reveals that local damage leads to relatively minor changes in the global eigenparameters, while the

Table 3 Simulated damage scenarios

Case	Damaged element	Reduction of bending rigidity
1	No. 33~35	−50%
2	No. 33~35	−80%
3	No. 85	−50%
4	No. 103 and 347	−50%, −60%

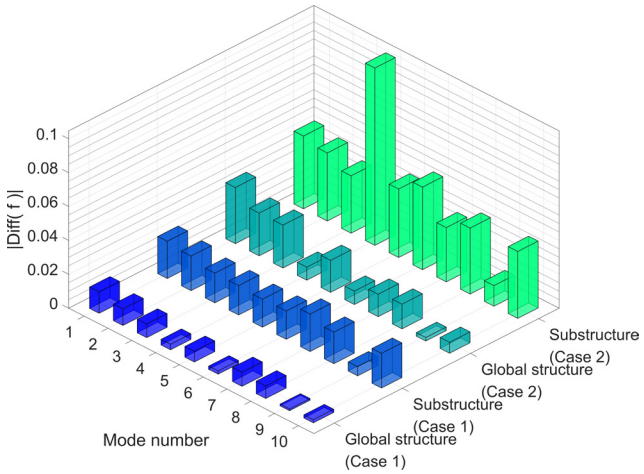

Fig. 7 Sensitivity of eigenparameters of global structure and substructure (Case 1 and 2)

same predetermined damage induces significant changes in the substructural eigenparameters. When the damage degree is at 50%, the relative change of the first 10 frequencies of the substructure generally falls around 0.02, with a maximum of 0.0221. The average of the first 20 MAC values of eigenvectors is 0.886. As the damage degree increases to 80%, the maximum relative frequency change of the substructure reaches 0.105, which is approximately 3.2 times higher than that of the global structure. The average of the first 20 MAC values of eigenvectors is 0.484.

From the analysis of the two damage conditions, it becomes evident that the eigenparameters of the substructure are more sensitive to damage compared to the global structure. Furthermore, the magnitude of change in eigenparameters caused by preset damage surpasses the error introduced by component mode synthesis, as shown in Scheme 3 of Fig. 5. Consequently, the proposed substructuring method exhibits significant advantages in damage identification for large-scale structures.

5 Numerical simulation of structural damage identification

5.1 Damage identification program

Establish the initial model and damage model using the MATLAB code [24], and write a damage identification program of substructure-based model updating. The program defines the Young's modulus of the structure as the updating parameter during the finite element model updating process. The specific steps are as follows:

1. Step 1: Structural decomposition:
   To effectively detect early structural damage and identify hidden risks, it is crucial to prevent local minor damages from being obscured by noise. This enables a comprehensive identification of structural damage and direct evaluation of its performance. One approach to achieve this is by employing the substructuring method, which involves dividing the entire structure into several substructures, as depicted in Fig. 3. The Stiffness matrix $\boldsymbol{K}$ and Mass matrix $\boldsymbol{M}$ of each substructure are assembled to analyze the modal properties of each substructure, such as the eigenvalue $\boldsymbol{\lambda}$, the lower order modes $\boldsymbol{\varphi}_l$, and the residual flexibility $\boldsymbol{\psi}$.
2. Step 2: Substructure-based model updating:
   Model updating is performed on the substructure by considering the first-order partial derivatives of the eigenvalues $\boldsymbol{\lambda}$ and eigenvectors $\boldsymbol{\varphi}$ with respect to the updating parameter $\boldsymbol{r}$, as described by Eqs. (29) and (40). These calculations contribute to the formation of the substructure sensitivity matrix $\boldsymbol{S}$. Since each substructure operates independently, parallel computation can be employed. Moreover, the updating parameter $\boldsymbol{r}$ is solely associated with the stiffness and mass matrices of the substructure that contains it, remaining unaffected by other substructures. Consequently, during the computation of the sensitivity matrix $\boldsymbol{S}$, substructures not containing the updating parameter $\boldsymbol{r}$ are assigned a sensitivity value of zero. By localizing damage and focusing on specific substructures, the number of unknown variables is significantly reduced, leading to a substantial improvement in model updating efficiency. The updating parameters are then reassembled, and the model properties of the substructure are recalculated following the modal updating process.
3. Step 3: Component mode synthesis:
   The modified substructures are assembled into diagonal blocks following Eq. (14), and the eigenparameters of the reorganized global structure are subsequently calculated using Eq. (21). Component mode synthesis technology is employed to reduce the analysis scale while preserving the modal properties of the structure. The frequency of a structure provides insight into its overall performance, while the modal shape reveals spatial and local information about the structure's vibration. Therefore, the objective function is formulated by considering the residuals of eigenvalue and eigenvector.
4. Step 4: Damage Identification:
   By performing multiple iterative operations, the structural parameters are continuously adjusted to mini-

mize the objective function. If the convergence conditions are not met, the substructure-based model updating program is revisited for further optimization until convergence is achieved. This iterative process enables the determination of the damage location and severity.

5.2 Damage identification based on substructure

The proposed substructure-based model updating method and the traditional model updating method are compared using measurement points arranged at each node, as indicated in Fig. 2. Damage identification is performed using the first 10 frequencies and modes, aiming to match the modal data of the updated model with the modal data of the damaged mode. The mode shapes are determined at the x and y direction of the nodes in Fig. 2. In the case 3, which the bending stiffness of element 85 (located in the first substructure) is reduced by 50%, the identified damage result is obtained by using the traditional global method after 64 iterations, as shown in Fig. 8. It successfully identified the preset damaged element 85, with a damage identification degree SRF of 44.02%.

On the other hand, the proposed substructure-based model updating method requires 132 iterations to reach convergence, and the identification results are presented in Fig. 9. The stiffness parameters of element 85 are reduced by 45.65%, and the reduction position of the stiffness parameters corresponds to the preset damage position. The relative error compared to the preset damage degree of 50% is only 8.7%, indicating a high level of accuracy in the identification process. The maximum SRF value for the remaining undamaged positions is only 2.62%, indicating a strong anti-interference capability. These results verify the successful identification of the location and degree of preset damage elements using the proposed substructure-based model updating method. Additionally, it was demonstrated that when employing scheme 3 based on the criterion of modal truncation, the error caused by CMS was negligible, and the proposed substructuring method proved effective in the model updating process.

In the fourth case, beam element 103 (located in the first substructure) and column element 347 (located in the second substructure) are preset to be damaged, with a reduction of 50% and 60% in their bending stiffness, respectively. The damage identification results are presented in Fig. 10 and Fig. 11. Both the proposed substructure-based

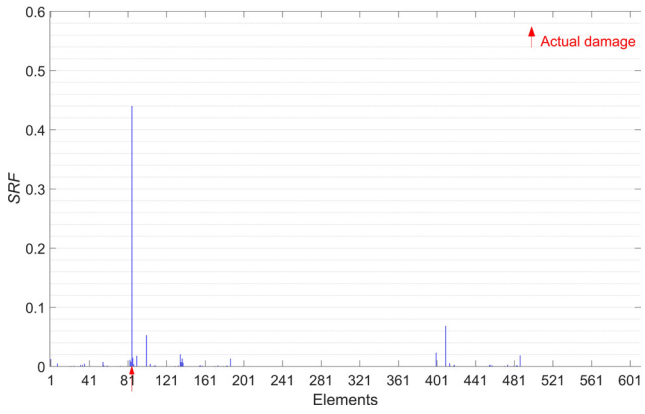

Fig. 8 Damage identification by global method (Case 3)

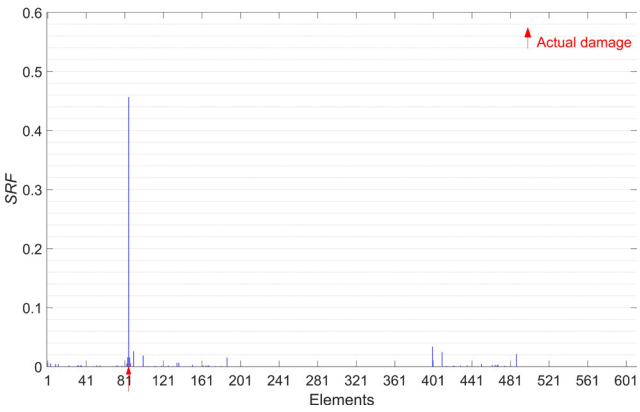

Fig. 9 Damage identification by substructuring method (Case 3)

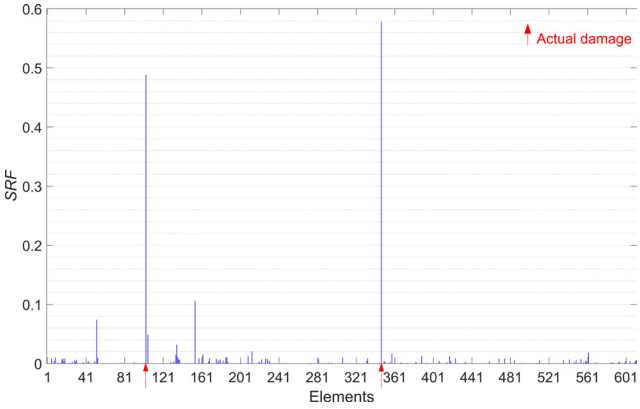

Fig. 10 Damage identification by global method (Case 4)

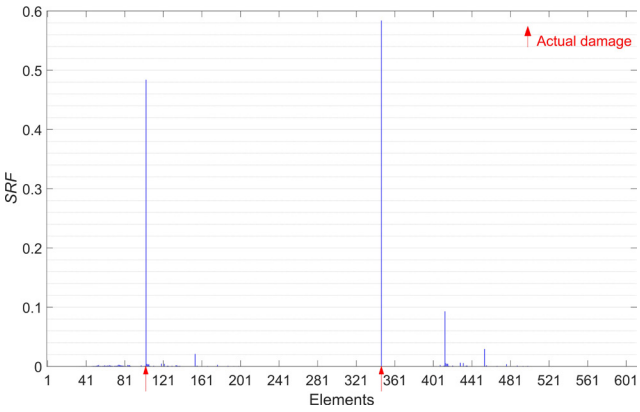

Fig. 11 Damage identification by substructuring method (Case 4)

method and the traditional method successfully detect damage, with the identified damage degree closely matching the preset damage degree. This further confirms the effectiveness of the proposed method. Table 4 compares the frequency and MAC values before and after the updated of Case 4. The results indicate that the modal data of the finite element model, modified based on the substructuring method, closely aligns with the data of the damaged structure. The relative differences in frequencies between the modified structure and the damaged structure are significantly reduced, with all values being less than 0.15%. The 2nd order MAC has increased from 0.8617 to 0.9923, indicating the accuracy of this method.

5.3 Computational efficiency

Table 5 presents the computational workload of the damage identification process and compares the matrix size, computational time, and number of iterations between the proposed substructure-based method and the global structural model updating method. The time required to calculate the eigenparameters using a complete finite element model is 47.3ms. In contrast, the calculation time of the eigenparameters based on the substructuring method is 29.3 ms, which is approximately 62% of the calculation time of the former. This indicates that the substructuring method can significantly improve the calculation efficiency while ensuring accuracy.

Regarding the efficiency of the model updating calculation, in case 3, the model updating method based on the global structure converges after 64 iterations and 4522.104 seconds, while the substructure-based model updating achieves convergence in only 1053.342 seconds, which is 23% of the time consumed by the former method. It is important to note that the matrix size based on the global structure is 1440, whereas the proposed substructuring method reduces the matrix size to 370. Therefore, compared to traditional methods, the substructuring method achieves a significant reduction in computational workload while maintaining model accuracy.

6 Conclusion

The iterative optimization algorithm used in finite element model updating often involves solving the eigensolutions of the global structural model multiple times. However, when dealing with large-scale finite element models that have a high number of degrees of freedom, a significant

Table 4 Frequencies and mode shapes before and after updating by substructure-based method (Case 4)

Mode No.	Damaged Freq.	Before updating			After updating		
		Freq. (Hz)	*Diff* (%)	MAC	Freq. (Hz)	*Diff* (%)	MAC
1	1.3401	1.3498	0.7238	0.9998	1.3407	0.0448	1.0000
2	1.4646	1.4858	1.4475	0.8617	1.4662	0.1092	0.9923
3	1.4719	1.4897	1.2093	0.8884	1.4733	0.0951	0.9951
4	1.9360	1.9480	0.6198	0.9997	1.9352	0.0413	0.9999
5	1.9576	1.9655	0.4036	0.9998	1.9563	0.0664	0.9999
6	2.5246	2.5313	0.2654	1.0000	2.5257	0.0436	1.0000
7	2.9479	2.9847	1.2483	0.9958	2.9516	0.1255	0.9989
8	3.0092	3.0144	0.1728	0.9999	3.0104	0.0399	1.0000
9	3.9703	4.0013	0.7808	0.9982	3.9742	0.0982	0.9997
10	4.1861	4.2270	0.977	0.9966	6.2657	0.1166	0.9989

Table 5 Comparison of computational efficiency

Computational efficiency	Simulated Damage Scenarios	Modal updating	
		Global method	Substructuring method
Size of eigensolutions		1440	370
Time consumed of eigensolutions (ms)		47.3	29.3
Iterations of modal updating	Case 3	64	132
	Case 4	92	172
Time consumed of modal updating/s	Case 3	4522.104	1053.342
	Case 4	6361.224	1442.483

number of updating parameters, and various environmental factors, the optimization process can encounter challenges such as slow convergence or even ill-conditioned problems. To address these issues, this article proposes a novel approach that utilizes component mode synthesis to divide large frame structures into several substructures. By focusing on model updating of the substructures rather than the entire structure, the accuracy and efficiency of the optimization process can be significantly improved. Moreover, this approach allows for a comprehensive evaluation of the structural safety throughout its entire lifespan by conducting critical area inspections. In summary, the proposed method offers valuable insights and solutions for the dynamic evaluation of large structures. The specific conclusions are as follows:

1. Traditional model updating methods applied to large structures face challenges due to the extensive number of parameters that need to be updating and the limited sensitivity of global structural dynamic parameters to local damage. In contrast, the proposed component mode synthesis method offers a more effective approach. By utilizing lower-order modal information from substructures, the analysis scale of the structure can be significantly reduced. The method compensates for higher-order modes using residual flexibility, ensuring accurate calculation of the main dynamic properties and sensitivity matrix of the structure. Furthermore, independent substructures, divided into localized regions, exhibit higher sensitivity to damage compared to the global structure. Consequently, the changes in eigenparameters resulting from preset damage are much more significant than the errors introduced by component mode synthesis.
2. The proposed substructuring method offers notable advantages in terms of computational efficiency and convergence speed compared to the traditional global model updating approach. Starting from the eigenequation, this article derives the sensitivity equation using the substructuring method, which facilitates the establishment of a damage identification program based on substructure model updating. One of the key advantages is the significant reduction in the scale of the system matrix, particularly the sensitivity matrix that requires element-by-element calculations. By leveraging simplified equations, the sensitivity matrix can be computed quickly. Additionally, during each iteration, only the derivative matrices of relevant independent substructures need to be calculated, while the derivative matrices of other substructures are set to zero. The substantial difference in computational workload greatly reduces the computational time required for model updating. Consequently, the proposed substructuring method achieves convergence in a shorter time compared to the traditional global model updating method.

Acknowledgement

The project presented in this article is supported by Natural Science Foundation of Fujian Province (Grant No. 2020J01942, 2021J011234), and University Young Research Talent Training Fund Project (Grant No. JXZ2017004).

References

[1] Matarazzo, T. J., Pakzad, S. N. "STRIDE for Structural Identification Using Expectation Maximization: Iterative Output-Only Method for Modal Identification", Journal of Engineering Mechanics, 142(4), 04015109, 2016. https://doi.org/10.1061/(ASCE)EM.1943-7889.0000951

[2] Fujino, Y., Siringoringo, D. M., Ikeda, Y., Nagayama, T., Mizutani, T. "Research and Implementations of Structural Monitoring for Bridges and Buildings in Japan", Engineering, 5(6), pp. 1093–1119, 2019. https://doi.org/10.1016/j.eng.2019.09.006

[3] Cheng, X.-X., Fan, J.-H., Xiao, Z.-H. "Finite element model updating for the Tsing Ma Bridge tower based on surrogate models", Journal of Low Frequency Noise, Vibration and Active Control, 41(2), pp. 500–518, 2022. https://doi.org/10.1177/14613484211058999

[4] Ni, Y. Q., Xia, Y., Lin, W., Chen, W. H., Ko, J. M. "SHM benchmark for high-rise structures: A reduced-order finite element model and field measurement data", Smart Structures and Systems, 10(4–5), pp. 411–426, 2012. https://doi.org/10.12989/sss.2012.10.4_5.411

[5] Li, Q., He, Y., Zhou, K., Han, X., He, Y., Shu, Z. "Structural health monitoring for a 600 m high skyscraper", The Structural Design of Tall and Special Buildings, 27(12), e1490, 2018. https://doi.org/10.1002/tal.1490

[6] Weng, S., Zhu, H., Xia, Y., Li, J.,Tian, W. "A review on dynamic substructuring methods for model updating and damage detection of large-scale structures", Advances in Structural Engineering, 23(3), pp. 584–600, 2020. https://doi.org/10.1177/1369433219872429

[7] Chen, H.-P. "Structural Health Monitoring of Large Civil Engineering Structures", Wiley Blackwell, 2018. ISBN 978-1-119-16643-6

[8] Bao, Y., Chen, Z., Wei, S., Xu, Y., Tang, Z., Li, H. "The State of the Art of Data Science and Engineering in Structural Health Monitoring", Engineering, 5(2), pp. 234–242, 2019. https://doi.org/10.1016/j.eng.2018.11.027

[9] Xia, Y., Hao, H. "Statistical damage identification of structures with frequency changes", Journal of Sound and Vibration, 263(4), pp. 853–870, 2003. https://doi.org/10.1016/S0022-460X(02)01077-5

[10] Mao, L., Weng, S., Li, S.-J., Zhu, H.-P.,Sun, Y.-H. "Statistical damage identification method based on dynamic response sensitivity", Journal of Low Frequency Noise, Vibration and Active Control, 39(3), pp. 560–571, 2020. https://doi.org/10.1177/1461348418784828

[11] Hou, R., Xia, Y. "Review on the new development of vibration-based damage identification for civil engineering structures: 2010–2019", Journal of Sound and Vibration, 491, 115741, 2021. https://doi.org/10.1016/j.jsv.2020.115741

[12] Bakir, P. G., Reynders, E., De Roeck, G. "Sensitivity-based finite element model updating using constrained optimization with a trust region algorithm", Journal of Sound and Vibration, 305(1–2), pp. 211–225, 2007. https://doi.org/10.1016/j.jsv.2007.03.044

[13] Yang, Y., Zhang, Y.,Tan, X. "Review on Vibration-Based Structural Health Monitoring Techniques and Technical Codes", Symmetry, 13(11), 1998, 2021. https://doi.org/10.3390/sym13111998

[14] Vaca Oyola, L. S., Jaime Fonseca, M. R., Rodríguez Rocha, R. "Damaged Flexibility Matrix Method for Damage Detection of Frame Buildings", Advances in Civil Engineering, 2020, 3534957, 2020. https://doi.org/10.1155/2020/3534957

[15] Shi, Z. Y., Law, S. S., Zhang, L. M. "Damage Localization by Directly Using Incomplete Mode Shapes", Journal of Engineering Mechanics, 126(6), pp. 656–660, 2000. https://doi.org/10.1061/(ASCE)0733-9399(2000)126:6(656)

[16] Wu, J. R., Li, Q. S. "Finite element model updating for a high-rise structure based on ambient vibration measurements", Engineering Structures, 26(7), pp. 979–990, 2004. https://doi.org/10.1016/j.engstruct.2004.03.002

[17] Weber, B., Paultre, P. "Damage Identification in a Truss Tower by Regularized Model Updating", Journal of Structural Engineering, 136(3), pp. 307–316, 2010. https://doi.org/10.1061/(ASCE)ST.1943-541X.0000105

[18] Papadimitriou, C., Papadioti, D.-C. "Component mode synthesis techniques for finite element model updating", Computers & Structures, 126, pp. 15–28, 2013. https://doi.org/10.1016/j.compstruc.2012.10.018

[19] Xia, Y., Hao, H., Deeks, A. J., Zhu, X. "Condition Assessment of Shear Connectors in Slab-Girder Bridges via Vibration Measurements", Journal of Bridge Engineering, 13(1), pp. 43–54, 2008. https://doi.org/10.1061/(ASCE)1084-0702(2008)13:1(43)

[20] Duan, Y. F., Xu, Y. L., Fei, Q. G., Wong, K. Y., Chan, K. W. Y., Ni, Y. Q., Ng, C. L. "Advanced Finite Eelement Model of Tsing Ma Bridge for Structural Health Monitoring", International Journal of Structural Stability and Dynamics, 11(2), pp. 313–344, 2011. https://doi.org/10.1142/S0219455411004117

[21] Craig, R. R.,Chang, C.-J. "Free-interface methods of substructure coupling for dynamic analysis", AIAA Journal, 14(11), pp. 1633–1635, 1976. https://doi.org/10.2514/3.7264

[22] Lu, Z. R., Law, S. S. "Features of dynamic response sensitivity and its application in damage detection", Journal of Sound and Vibration, 303(1-2), pp. 305–329, 2007. https://doi.org/10.1016/j.jsv.2007.01.021

[23] Nelson, R. B. "Simplified calculation of eigenvector derivatives", AIAA Journal, 14(9), pp. 1201–1205, 1976. https://doi.org/10.2514/3.7211

[24] MathWorks Inc "MATLAB, R2021a", [online] Available at: https://www.mathworks.com/help/matlab/release-notes-R2021a.html [Accessed: 19 October 2023]

[25] Ansys Inc "Ansys, 2020 R2", [online] Available at: https://www.ansys.com/resource-center/brochure/ansys-release-capabilities [Accessed: 19 October 2023]